Solid State Transformer based on Grain-Oriented Electrical Steel Wound Cores

Sidi Hamdinou, Daniel Roger, Mathieu Rossi, Thierry Belgrand

Solid State Transformer based on Grain-Oriented Electrical Steel Wound Cores

*

1st Sidi Hamdinou
LSEE
Université d'Artois
Bethune, France
shamdinou.hamdinou@univ-artois.fr

2nd Daniel Roger
LSEE
Université d'Artois
Bethune, France

3th Mathieu Rossi
LSEE
Université d'Artois
Bethune, France

4rd Thierry Belgrand
thyssenkrupp Electrical Steel
Isbergues, France
Thierry.belgrand@thyssenkrupp.com

***Abstract*—Considering the progress in semi-conductor technology and magnetic core material performances, an increased attention is paid to the so called Solid-State Transformers (SST). Besides the ability to monitor the direction of the power flow compared to classical 50/60 Hz transformers, these devices, composed of power converters placed each side of a high frequency power transformer, offer many advantages such as small size and low weight.**

The main focus of this paper is to report about the transformer itself as a key element of the SST. Thin grain oriented electrical steel (GOES) has been chosen for building the core of the transformer. Reasons for this choice are the high saturation polarization capability even at high temperature and its availability on a large scale compared to amorphous and nanocrystalline materials used in current SSTs; thus thin GOES seems to be a good alternative to achieve a technological and economical balance by playing on both frequency and working induction levels to reduce the size of the transformer.

The aim of the study is to assess the limits of the GOES use in terms of maximum operating frequency and flux density for power electronic like voltages, offering both high power density and efficiency in reduced volume.

The primary and secondary windings of the transformer are respectively connected to standard electronic converters that deliver square shaped voltages. Losses under such regimes far from classical sinus cases have to be assessed. They are the root cause for heating of the device and shall be known before energizing the transformer. Experimental results and finite-element simulation performed on the core structure, show that dynamic core losses are lower for square wave voltages than for sine waves at the same peak flux density and frequency.

The maximum winding operating temperature obtained at thermal equilibrium fixes the operating limits of the device. Then to avoid issues due to eventual overheating when energizing the transformer, a thermal model suitable for predicting the temperature at various transformer locations has been developed and used; results are then described.

***Index Terms*—Medium Frequency, Power transformer, Grain oriented Electrical steel, Transformer losses, Power electronics**

I. Introduction

Solid-State transformers (SST) are promising technologies for future electrical DC grids [1]. The basic topology of SST is made of two power electronic converters linked via a medium or high frequency transformer (Fig.1). This structure is adapted to smart grids and clean technologies [2], [3].Several topologies of SSTs are available for various applications [4].

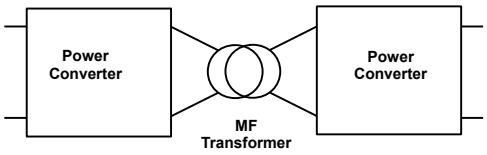

Fig. 1. Basic topology of SST

The transformer is one of the main components of the SST; it ensures the energy transfer as well as the voltage change with a galvanic separation between input and output stages. Because of high operating frequencies, the volume of the transformer is reduced compared to same rated power transformers working at 50/60 Hz.

A big challenge in the SST design process stands in reaching at the same time high efficiency and power density at a reasonable cost. To such extent, optimization process has to consider the nature and quality of the magnetic materials, the power electronic components, the switching strategy and the drivers [5].

In most of the reported cases [6]–[8], SSTs combine amorphous or nano-crystalline magnetic materials for the core and wide-bandgap semiconductors together with complex control strategies. These structures are preferably used at frequencies above 10 kHz.

Well established silicon-based IGBT converters combined to wide-spread thin GOES having high saturation polarization and high temperature operating capability may offer the opportunity for simpler and more cost effective solutions for the design of high power SSTs. SSTs are used to convert DC to DC voltages. The voltage change is made via a conversion of DC voltage into square wave voltage to feed the transformer core. In case of simple square waves voltages, the dynamic core losses show lower levels compared to the case of sine

waves at same maximum flux density and frequency. The figures of the experimental result are illustrated using proper finite elements simulations for various experienced wound core cases.

The aim of the study is to assess the limits of the use of GOES wound core for SST applications. Due to the inorganic nature of its insulating layer, GOES can be operated up to around 400°C with little loss in its magnetization ability. This has to be considered for experiencing first the limits of the operating conditions then the maximum power that can be transmitted through a given volume of wound core, and finally the efficiency. All these parameters can only be known once the thermal equilibrium has been reached.

Decreasing the transformer size results into an increase in loss density which may be critical for the winding temperature with regards to its insulation class. Therefore, an efficient cooling system is compulsory if the core is to be pushed to its full capacity. A thermal model has been built in order to predict the temperature at all the transformer parts, depending on the operating conditions. This is meant to prevent from any safety issue like the one induced by a fire of the set up.

The paper focuses on a the magnetic and thermal behaviour of a medium-frequency thin GOES core transformer (MFGO) prototype. First of all a suitable method using 2D finite elements model has been settled to be able to compute properly the flux density and eddy currents distributions within the transformer core. This was proved necessary in order to estimate at best the core losses. As a complement for optimization of the transformer structure, a thermal model is described.

II. Finite Elements (FE) simulation

In this section two ways of simulating the magnetic behavior of the core geometry are presented taking into account the non-linearity of the core material magnetic property. They differ by the representation of the geometry and the application of the boundary conditions. One shows limitations which are generally overcome by using homogenization techniques applied to the laminated structure.The other one proves to be more representative of the real case. An open source software called GMSH [9]associated to Getdp solver [10] have been used to perform the simulations.

A. Classical FE model

Fig.2 shows a stack of laminations that can be seen as a part of the wound core for which the rolling direction of the electrical steel is oriented along the Y axis. For the sake of simplicity of the model the geometry is made of three laminations, each one having a width of 0.165 mm. The boundary conditions are defined by the magnetic vector potential Az in the Oz direction corresponding to a magnetization along the Y axis (easy magnetization axis of GOES) . The vector potential is defined by :

$$\vec{B} = \vec{curl}\left(\vec{A}\right) \tag{1}$$

Imposing A is equivalent to monitor the transformer voltage, therefore it avoids any need for coupling the FEM with an external electrical circuit. The problem is then formulated by the magnetic vector potential [13].

The simulation results are presented by Fig.3 It shows a screening effect which hinders the magnetic flux to go deep inside the laminated structure. The edge laminations channel the whole magnetic flux and the center lamination reminds free of flux density. This result is due to 2D modelling with an infinite z-axis along which the induced currents flows and never buckles to form a closed loop.

To overcome this limitation, it is of common practice to use homogenization principle [11], [12], however this approach is used to simulate only one operating condition. In the reported case, non-linearities and time dependencies are to be considered. Thus space-time evolution of the flux density and eddy currents are needed. Therefore, an alternative solution is proposed.

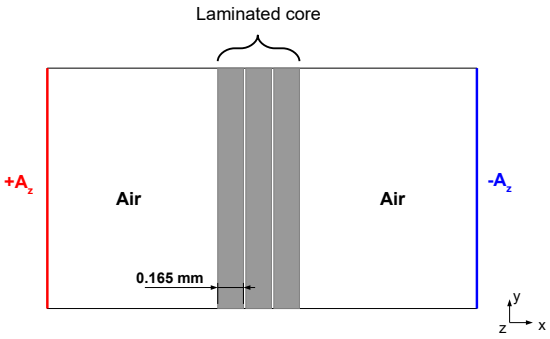

Fig. 2. 2D model of laminated core

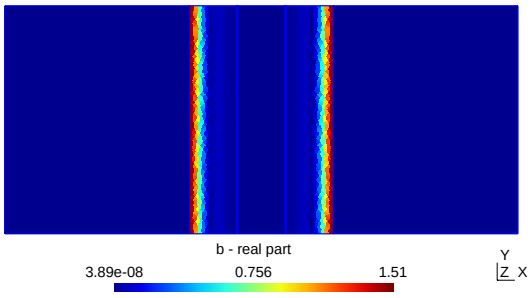

Fig. 3. Simulation results of the classical approach, flux density at 2 kHz

B. Alternative FE model

Now the representation of the structure is moved such as RD is perpendicular to the plane (Oz axis). This correspond to a view of the magnetic circuit from above the horizontal airgap separating the two halves of one half core (Fig. 4), the thickness of the laminations composing the wound core being along the X axis and the width of the lamination being along the Y axis (Fig.4). The vector potential A is located in the x-y plane; B is along the Oz direction, parallel to RD. The formulation is expressed in terms of polar coordinate (2),

$$\frac{1}{r}\left(\frac{\partial}{\partial r}\left(rA_\theta\right)-\frac{\partial A_r}{\partial \theta}\right)=B_z\left(r,\theta\right) \tag{2}$$

Results of simulation in linear magneto-harmonics are represented in Fig.5 where it can be seen that the distribution of the magnetic flux density is the same whatever the position of the lamination.

Considering this result, we assume that the distribution of the magnetic flux density and eddy currents is the same along the wound core (Fig.6).

Therefore, we propose a more simple model where we consider, this time, a limited length of one core lamination along RD; in this case, the thickness of the lamination is along X axis, and its width is along Z axis. The potential A is applied along Z direction, corresponding to a flux density in the 0x-0y plane. The extract of the Fig.6 shows the representation of the model. This model which principle is the same as described in section A but for a single lamination, favours more time calculation saving when non-linearity and time dependence are taken into account.

The obtained result for this limited length of lamination is propagated to the whole core dimension by proper translation operations.

The calculation at post-processing stage is then, using the following formulas, (3) is for instantaneous losses, and (4) is for average losses:

$$p_e\left(k\right)=N_s\times L_m\times L_z\times\sum\rho J_e^2\left(k\right)\Delta x \tag{3}$$

$$Pe=\frac{1}{T}\sum p_e\left(k\right)\Delta T \tag{4}$$

N_e : number of laminations within the core; L_m : Average magnetic path Length (m); L_z : core width (m)

A more strict formulation would be using an individual L_m for the field circulation along each individual turn of the wound laminations; but for the sake of simplicity at getting a good order of magnitude of P_e, an average L_m has been preferably considered.

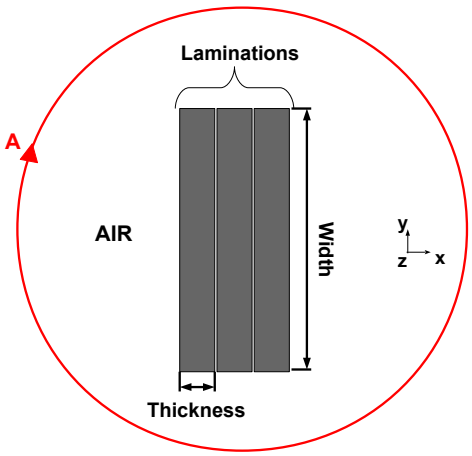

Fig. 4. 2D cross-sectional model

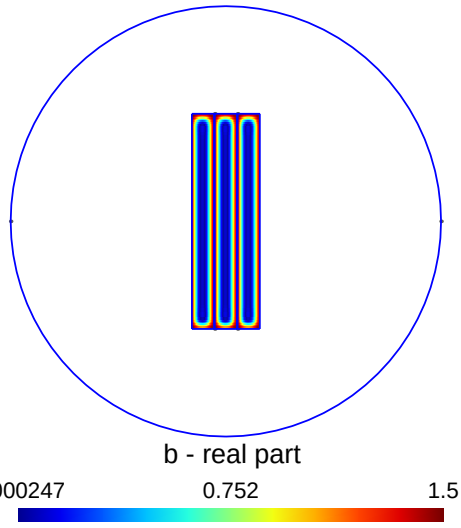

Fig. 5. simulation results : flux density distribution at 2 kHz

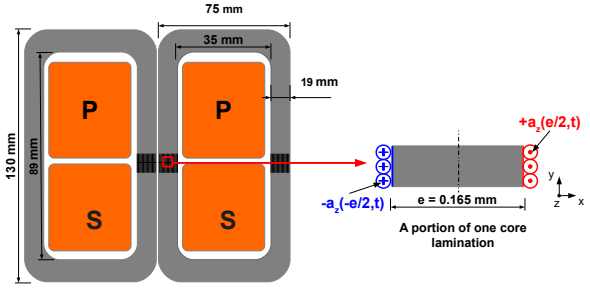

Fig. 6. Geometry of the magnetic core and windings and extract view of one lamination

C. Discussion

In the first place, simulation is ran for triangular vector potential (square wave voltage) on boundaries using the one length limited lamination model described in section II-B, the frequency of the signal is 2 kHz. Similarly, in a second step a sinusoidal vector potential (sinusoidal voltage) has been set to get the same conditions for comparison.

The Fig.7 shows the distribution of flux density at 2 kHz and for an imposed triangular potential vector A on the edges in order to get an average flux of $1.5\,T$ as peak value.

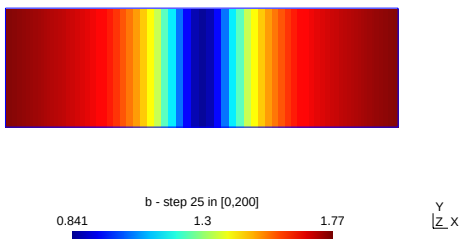

Fig. 7. Distribution of flux density at 2 kHz, average $B_{max}=1.5\,T$ in case of imposed triangular potential vector on the edges

Results of losses calculation are presented in table I; they show that the losses under square wave voltage (triangular vector potential) are lower than under sinusoidal voltage for the same peak magnetic flux density.

TABLE I
EDDY CURRENT LOSSES CALCULATION

	Triangular A (Square Volatge)		Sinusoidal A (Sinusoidal Voltage)	
Losses at 2 kHz	1 T	1.5 T	1 T	1.5 T
	65 W	197.5 W	81 W	231 W

This result is against the prevailing idea which is that under sinusoidal excitation, losses are lower than under square wave one. This belief is associated to the consideration of losses coming out from a sum of sinusoidal harmonic contributions according to Fourier principle; but this is not a worthy assumption since the engaged phenomenon are not linear (material characteristic) and Fourier principle applies only for linear cases.

Experimentation results reported hereafter brings the necessary validation to the computed results.

D. Experimentation

Experimentation is performed on the prototype shown in Fig.8. The conductor windings is made of $100 \times 0.5mm$ parallel connected high temperature withstanding wires. The insulation between the winding and the core is ensured by glass fiber tapes also able to withstand high temperatures. Core losses under square and sinusoidal voltages are measured at no load, the results are presented in the table II.

Fig. 8. Transformer prototype

TABLE II
COMPARISON OF MEASURED CORE LOSSES

	1 kHz		2 kHz
	1 T	1.5 T	1 T
Square voltage	56 W	118 W	168 W
Sine Voltge	60 W	129 W	196 W

The experimental results confirm that under square wave voltage losses are lower than sinusoidal voltage; the differences observed between simulation and experiment is due to the fact that simulation only accounts for eddy currents. No hysteresis loss neither excess loss as well as the building factor due to change in magnetic properties associated to building process have been considered in the simulation.

III. THERMAL MODEL

The thermal equilibrium is a key point for assessing the maximum operating conditions, and the maximum transmitted power across the transformer. By increasing the operating frequency and flux density, the losses density induce a temperature rise of the transformer core. A thermal model is compulsory to simulate the performance and to find out the optimal operating point of the transformer.

Therefore we propose a simple static model, based on the following assumptions:

- Uniformity of the temperature inside the core and the windings, because of the high thermal conductivity of copper and steel.
- Heat transfer mainly occurs by conduction and convection mechanisms.
- Thermal conductivity is independent from temperature.
- Thermal exchange between the primary and secondary windings is neglected, because of their structures and positions, this assumption is supported by the experimental results

A. Presentation of the model

The equivalent circuit of the model, based upon the above assumptions, is shown in Fig.10 where P_c and P_w are respectively the core and the winding total losses (W). T_c , T_p, T_s and T_a are respectively the core, the primary, the secondary windings and the air temperatures (°C).

The model is described by the following system of linear equations :

$$\begin{cases} P_c = & G_{cp}\left(T_c - T_p\right) + G_{cs}\left(T_c - T_s\right) + G_{ca}\left(T_c - T_a\right) \\ P_p = & G_{cp}\left(T_p - T_c\right) + G_{pa}\left(T_p - T_a\right) \\ P_s = & G_{cs}\left(T_s - T_c\right) + G_{sa}\left(T_s - T_a\right) \end{cases} \tag{5}$$

Which can be written under the of a matrix as follow :

$$[P]_{3\times1} = [A]_{3\times3}\,[T]_{3\times1} + [B]_{3\times1}\,T_a \tag{6}$$

where :

$$[P] = \begin{bmatrix} P_c \\ P_p \\ P_s \end{bmatrix}; \quad [T] = \begin{bmatrix} T_c \\ T_p \\ T_s \end{bmatrix}; \quad [B] = \begin{bmatrix} -G_{ca} \\ -G_{ca} \\ -G_{ca} \end{bmatrix}$$

$$[A] = \begin{bmatrix} G_{cp} + G_{cs} + G_{ca} & -G_{cp} & -G_{ca} \\ -G_{cp} & G_{cp} & 0 \\ -G_{cs} & 0 & G_{cs} + G_{sa} \end{bmatrix};$$

The model predicts the temperatures by solving the (6); as following :

$$[T] = [A]^{-1}\left([P] - [B]\,T_a\right) \tag{7}$$

However, thermal conductances must be first calculated. For that purpose an experimental method is proposed. It is based on performing various tests and direct measurements of the

temperatures with thermocouples placed at various locations of the transformer. The locations are shown by Fig.9 and described in table III.

Three tests are conducted the transformer being cooled by a forced airflow of $325\,m^3/h$; the tests are: a no-load condition test, a DC test in the primary, and a DC test in the secondary.

These tests allow us to write the system of equations (8) using (5) :

TABLE III
THERMOCOUPLES POSITIONS

Thermocouples	Position
T1	In contact with the left core
T2	In contact with the right core
T3	Primary between wires
T4	Primary between turns
T5	Secondary between wires
T6	Secondary between turns
T7	Air above the transformer
T8	Air below the transformer

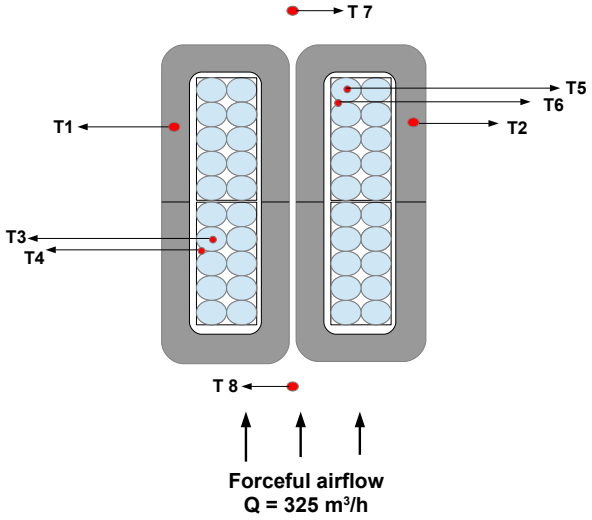

Fig. 9. Positions of thermocouples used for tests

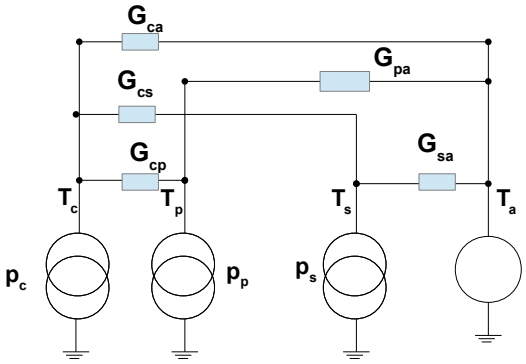

Fig. 10. Thermal equivalent circuit

$$\begin{cases} P_c = & G_{cp}\left(T_c^1 - T_p^1\right) + G_{cs}\left(T_c^1 - T_s^1\right) + G_{ca}\left(T_c^1 - T_a^1\right) \\ P_p = & G_{cp}\left(T_c^2 - T_p^2\right) + G_{cs}\left(T_c^2 - T_s^2\right) + G_{ca}\left(T_c^2 - T_a^2\right) \\ P_s = & G_{cp}\left(T_c^3 - T_p^3\right) + G_{cs}\left(T_c^3 - T_s^3\right) + G_{ca}\left(T_c^3 - T_a^3\right) \end{cases} \tag{8}$$

The system (8) allows us to calculate the conductances G_{ca}, G_{pa}, G_{sa}; G_{cp}, and G_{cs} are calculated using the following equations from no-load test :

$$\begin{cases} G_{cp} = & \frac{T_p - T_a}{T_c - T_a} G_{pa} \\ G_{cs} = & \frac{T_s - T_a}{T_c - T_a} G_{sa} \end{cases} \tag{9}$$

B. Model calculations

The obtained results are summarized in table IV. Fig. 11 and 12 show the temperatures evolution at the various transformer locations in no-load and DC tests. At no-load the windings are mainly heated by the thermal exchange with the core and their respective temperatures are slightly different from each other. This is due to the fact that hot air flowing from beneath as pushed by the fan brings heat to the secondary winding in upper position. In the DC test the primary winding got heated by Joule losses, however the secondary winding temperature had changed slightly against the air temperature. These two observations lead to the assumption that the thermal exchange between primary and secondary windings is relatively low and can be neglected to simplify the model.

Computed results are presented in table V under the form of thermal resistances $R = \frac{1}{G}$.

To assess the accuracy of the model, measured temperatures and simulated ones are compared for two different situations, the results are presented in table VI. Since the computed figures are nearby the measured one, the model can be considered as a fair representation of the real situation.

TABLE IV
TESTS RESULTS

	P_c (W)	T_c ($^\circ C$)	T_p ($^\circ C$)	T_s ($^\circ C$)	T_a ($^\circ C$)
No-Load test $f = 2\,kHz$, $B_{max} = 1.5\,T$	274	153	60	65	28
DC test primary $I_{DCP} = 45A$	35.5	23	36.5	24	22.5
DC test secondary I_{DCS}=56 A	49	24.5	24.3	42	24

TABLE V
THERMAL RESISTANCES VALUES

R_{ca}	R_{pa}	R_{sa}	R_{cp}	R_{sp}
$1.1\,^\circ C/W$	$0.46\,^\circ C/W$	$0.4\,^\circ C/W$	$1.4\,^\circ C/W$	$0.9\,^\circ C/W$

C. simulation results

The model is used to simulate the transformer behavior on load at different operating frequencies in order to assess the limits of GOES use for SSTs applications.

The simulation results are summarized in table VII. It shows that maximum operating frequency and flux density, with

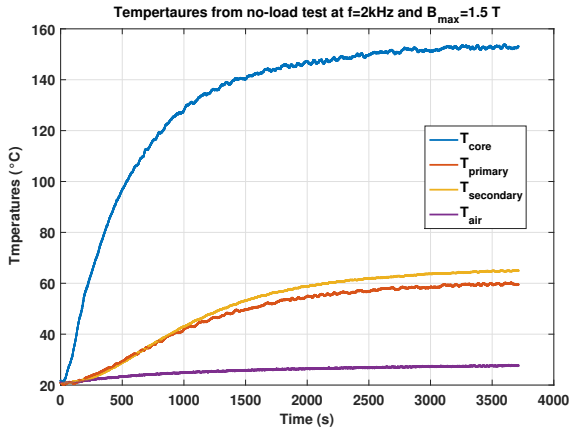

Fig. 11. No-load test temperatures

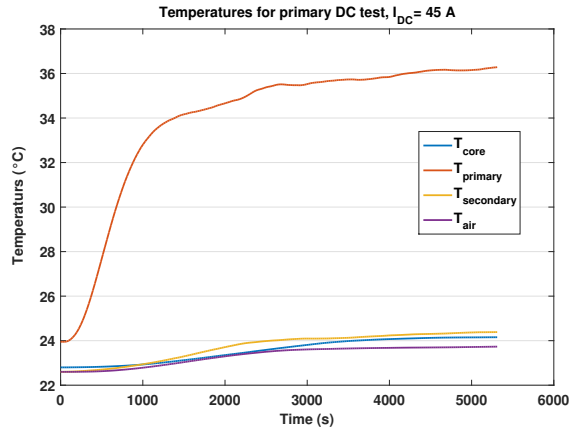

Fig. 12. Primary DC test temperatures

TABLE VI
MODEL VERIFICATION

	No-load test : $3\,kHz$ and $B_{max} = 1.5T$		Short-circuit test : $2\,kHz$ and $I_{sc} = 30\,A$	
	Measures	Simulation	Measures	Simulation
T_c	$233\,°C$	$249\,°C$	$25.5\,°C$	$31\,°C$
T_p	$96\,°C$	$86\,°C$	$41\,°C$	$36\,°C$
T_s	$104\,°C$	$96\,°C$	$36\,°C$	$33.5\,°C$
T_a	$33\,°C$		$23\,°C$	

TABLE VII
SIMULATION RESULTS OF LOAD TEST USING THE THERMAL MODE

Test	T_c	T_p	T_s	P_{max} Transmissible	Max. efficiency
$2kHz$ $1.5T$	$186°C$	$111C$	$111°C$	$6kW$	91%
$3kHz$ $1.5T$	$303°C$	$176°C$	$176°C$	$10.6kW$	92%
$4kHz$ $1.5T$	$647°C$	$358°C$	$360°C$	$17kW$	89

regards to the thermal limitation in the chosen reduced volume case, is 3 kHz and 1.5 T. In the case of an applied voltage of $160\,V$, the maximum transmitted power is about $10.6\,kW$ and the efficiency 92%. The transformer prototype having a core weight of $2\,kg$ this means that a power density of $5.3\,kW/kg$ has been achieved.

The result would be furthermore improved by boosting the cooling system and optimizing the windings configuration to better fill in the window of the core.

IV. Conclusion

It has been shown the performances of a medium frequency power transformer concept using thin grain oriented electrical steel. The experienced transformer prototype is able of $3\,kHz$ and $1,5\,T$ operation under power electronic like voltages for a power density of $5\,kW/kg$ associated to a simple cooling system. An improved cooling and adapted winding lay out would improve further on those performances. The obtained results are consistent with the development of such concept for potentially offering simple and reliable technology along with optimum technical economic solutions to the market.

References

[1] X. She and A. Huang, "Solid state transformer in the future smart electrical system," 2013 IEEE Power Energy Society General Meeting, Vancouver, BC, 2013, pp. 1-5. doi: 10.1109/PESMG.2013.6672768

[2] B. Liu, Y. Zha, T. Zhang and S. Chen, "Solid state transformer application to grid connected photovoltaic inverters," 2016 International Conference on Smart Grid and Clean Energy Technologies (ICSGCE), Chengdu, 2016, pp. 248-251. doi: 10.1109/ICSGCE.2016.7876063

[3] F. Bignucolo, M. Bertoluzzo and C. Fontana, "Applications of the solid state transformer concept in the electrical power system," 2015 AEIT International Annual Conference (AEIT), Naples, 2015, pp. 1-6. doi: 10.1109/AEIT.2015.7415235

[4] S. Falcones, X. Mao and R. Ayyanar, "Topology comparison for Solid State Transformer implementation," IEEE PES General Meeting, Providence, RI, 2010, pp. 1-8. doi: 10.1109/PES.2010.5590086

[5] O. A. Hassan, C. Klumpner and G. Asher, "Design considerations for core material selection and operating modes for a high frequency transformer used in an isolated DC/DC converter," Proceedings of the 2011 14th European Conference on Power Electronics and Applications, Birmingham, 2011, pp. 1-11.

[6] C. Zhao et al., "Power Electronic Traction Transformer—Medium Voltage Prototype," in IEEE Transactions on Industrial Electronics, vol. 61, no. 7, pp. 3257-3268, July 2014. doi: 10.1109/TIE.2013.2278960

[7] T. Zhao, L. Yang, J. Wang and A. Q. Huang, "270 kVA Solid State Transformer Based on 10 kV SiC Power Devices," 2007 IEEE Electric Ship Technologies Symposium, Arlington, VA, 2007, pp. 145-149. doi: 10.1109/ESTS.2007.372077

[8] X. She, A. Q. Huang and R. Burgos, "Review of Solid-State Transformer Technologies and Their Application in Power Distribution Systems," in IEEE Journal of Emerging and Selected Topics in Power Electronics, vol. 1, no. 3, pp. 186-198, Sept. 2013. doi: 10.1109/JESTPE.2013.2277917

[9] Geuzaine, C., Remacle, J. F. (2009). Gmsh: A 3-D finite element mesh generator with built-in pre-and post-processing facilities. International journal for numerical methods in engineering, 79(11), 1309-1331.

[10] Dular, P., Geuzaine, C. (1997). GetDP: A general environment for the treatment of discrete problems.

[11] , Johan, GEUZAINE, Christophe, et SABARIEGO, Ruth. Considering laminated cores and eddy currents in 2D and 3D finite element simulation of electrical machines. 2011.

[12] NEUBERT, Holger, ZISKE, Johannes, HEIMPOLD, Tobias, et al. Homogenization Approaches for Laminated Magnetic Cores using the Example of Transient 3D Transformer Modeling. In : Proc. of the 7th European COMSOL Conference, 23.-25.10. 2013, Rotterdam, NL. 2013.

[13] BASTOS, João Pedro A. et SADOWSKI, Nelson. Electromagnetic modeling by finite element methods. CRC press, 2003.